

The single photon sensitivity of the Adaptive Gain Integrating Pixel Detector

Julian Becker^{a,*}, Dominic Greiffenberg^b, Ulrich Trunk^a, Xintian Shi^b, Roberto Dinapoli^b, Aldo Mozzanica^b, Beat Henrich^b, Bernd Schmitt^b, Heinz Graafsma^a

^aDeutsches Elektronen-Synchrotron,
Notkestr. 85, 22607 Hamburg
^bPaul Scherrer Institute,
5232 Villigen PSI, Switzerland

Abstract

Single photon sensitivity is an important property of certain detection systems. This work investigated the single photon sensitivity of the Adaptive Gain Integrating Pixel Detector (AGIPD) and its dependence on possible detector noise values. Due to special requirements at the European X-ray Free Electron Laser (XFEL) the AGIPD finds the number of photons absorbed in each pixel by integrating the total signal. Photon counting is done off line on a thresholded data set.

It was shown that AGIPD will be sensitive to single photons of 8 keV energy or more (detection efficiency $\gg 50\%$, less than 1 count due to noise per 10^6 pixels). Should the final noise be at the lower end of the possible range (200 - 400 electrons) single photon sensitivity can also be achieved at 5 keV beam energy.

It was shown that charge summing schemes are beneficial when the noise is sufficiently low. The total detection rate of events is increased and the probability to count a single event twice in adjacent pixels is reduced by a factor of 40.

The entry window of AGIPD allows 3 keV photons to reach the sensitive volume with approximately 70% probability. Therefore the low energy performance of AGIPD was explored, finding a maximum noise floor below 0.035 hits/pixel/frame at 3 keV beam energy. Depending on the noise level and selected threshold this value can be reduced by a factor of approximately 10. Even though single photon sensitivity, as defined in this work, is not given, imaging at this energy is still possible, allowing Poisson noise limited performance for signals significantly above the noise floor.

Keywords: AGIPD, simulation, European XFEL, noise performance

1. Introduction

The European X-Ray Free Electron Laser (XFEL) [1, 2] will provide ultra short, highly coherent X-ray pulses which will revolutionize scientific experiments in a variety of disciplines spanning physics, chemistry, materials science, and biology.

One of the differences between the European XFEL and other free electron laser sources is the high pulse repetition frequency of 4.5 MHz. The European XFEL will provide pulse trains, consisting of up to 2700 pulses separated by 220 ns (600 μ s in total) followed by an idle time of 99.4 ms, resulting in a supercycle of 10 Hz and 27000 pulses per second.

Dedicated fast 2D detectors are being developed, one of which is the Adaptive Gain Integrating Pixel Detector (AGIPD) [3, 4, 5]. This development is a collaboration between DESY, the University of Hamburg, the University of Bonn (all in Germany) and the Paul Scherrer Institute (PSI) in Switzerland.

Many experiments at the European XFEL will require single photon sensitivity, which is an important requirement of the detection system. Due to the large variety of experiments foreseen at the European XFEL one cannot define a unique requirement for all experiments, but rather one has to optimize performance parameters like the number of noise counts/pixel/frame (false positive rate) and single photon detection efficiency (true positive rate) with respect to each individual experiment.

In this study, single photon sensitivity of AGIPD is defined as a false positive rate is below 10^{-6} (less than one hit due to noise per frame of 1 mega pixel) while simultaneously having an average true positive rate of more than 50%. The single photon sensitivity is investigated for the design energy of 12.4 keV and the optional lower operating energies of 8, 5 and 3 keV [6, 7].

2. The Adaptive Gain Integrating Pixel Detector (AGIPD)

AGIPD is based on the hybrid pixel technology. The current design goals of the newly developed Application Specific Integrated Circuit (ASIC) with dynamic gain switching amplifier in each pixel are (for each pixel) a dynamic

*Corresponding author

Email address: Julian.Becker@desy.de (Julian Becker)

42 range of more than 10^4 12.4 keV photons in the lowest 87
 43 gain, single photon sensitivity in the highest gain, an ana- 88
 44 log memory capable of storing 352 images, and operation 89
 45 at 4.5 MHz speed. A vetoing scheme allows to maximize 90
 46 the number of useful images that are acquired by providing 91
 47 the possibility to overwrite any previously recorded image 92
 48 during the pulse train.

49 Due to the special pulse structure of the European 93
 50 XFEL, it is necessary to store the acquired images inside 94
 51 the pixel logic during the pulse train. A compromise had 95
 52 to be found between storing many images, requiring a large 96
 53 pixel area, and high spatial resolution, requiring small pix- 97
 54 els sizes [3, 4].

55 The AGIPD will feature a pixel size of $(200 \mu\text{m})^2$ and a 98
 56 silicon sensor with a thickness of $500 \mu\text{m}$. The image data 99
 57 is read out and digitized in the 99.4 ms between pulse 100
 58 trains. 101

59 3. Performance parameters 102

60 Single photon sensitivity is determined by a number of 103
 61 parameters. The most important of these are the equiva- 104
 62 lent noise charge (ENC) of the system and the threshold 105
 63 Th , defining events above threshold as 'hit' (1)¹ and events 106
 64 below as 'no hit' (0). 107

65 First of all there is the probability to detect a photon 108
 66 which has interacted² in the sensor. This probability of a 109
 67 true positive $P(1|1)$ should be as high as possible, not to 110
 68 loose events. As long as the difference between the signal 111
 69 level S and the threshold is on the order of the noise 112
 70 ($S - Th \approx O(ENC)$) decreasing the threshold increases 113
 71 $P(1|1)$. 114

72 Another key performance parameter is the number of 115
 73 false positives $P(1|0)$ per pixel per frame. A false positive 116
 74 is defined as a pixel with a signal above threshold, although 117
 75 there are no photons impinging on the sensor. The number 118
 76 of false positives N_{false} can be easily measured by acquir- 119
 77 ing dark images. Assuming Gaussian distributed random 120
 78 noise in a pixel, a reasonable approximation is: 121

$$79 \quad N_{false} = 0.5 N_{pix} \operatorname{erfc} \left(\frac{Th}{\sqrt{2} ENC} \right), \quad (1)_{124}$$

80 where N_{pix} is the number of detector pixels and $\operatorname{erfc}(x)$ the 125
 81 complementary error function. As long as $Th \approx O(ENC)$ 126
 82 increasing the threshold decreases $P(1|0)$, and an accept- 127
 83 able balance between false and true positive rate has to be 128
 84 found. 129

85 Charge sharing and in-sensor scattering may cause an 130
 86 event not being detected in the pixel where its primary 131
 132
 133

interaction took place. Therefore two additional perfor-
 mance parameters are of interest: The expected number
 of pixels above threshold surrounding a pixel in which a
 primary event took place (neighboring events), and the
 additional number of events created in the local neighbor-
 hood (double counts).

4. HORUS

The detector response was calculated using the HO-
 RUS software described in [5, 8]. HORUS has already
 been successfully used to simulate the performance of the
 Medipix3 chip [9, 10] and recently for AGIPD [11, 12]. For
 this study HORUS has been upgraded to include the simu-
 lation of the K-edge fluorescence of silicon, elastic (Thom-
 son or Rayleigh) scattering and inelastic (Compton) scat-
 tering within the sensor material.

4.1. Validation of simulation results

A set of measurements using an assembly of AGIPD02
 was compared to corresponding simulations in order to
 validate the HORUS package.

The measurements were performed using a copper an-
 ode X-ray tube³ illuminating a high purity⁴ molybdenum
 foil. The detector assembly was positioned at 90° angle
 with respect to the X-ray beam from the tube (the foil
 was positioned at 45° with respect to each) in order to
 minimize the elastically scattered photons from the x-ray
 beam. The distance between foil and assembly was about
 15 cm, so effects of non-perpendicular photon incidence
 were minimal. The detector assembly was mounted in a
 custom made chip tester box that handled all communi-
 cation with the ASIC. In contrast to the sensor thickness
 intended for the full scale detector, the ASIC was bump
 bonded to a silicon sensor of $320 \mu\text{m}$ thickness having a
 depletion voltage of approximately 50 V. To (over-)deplete
 the sensor a bias voltage of 120 V was applied. All mea-
 surements were performed without cooling at room tem-
 perature. Due to the power dissipation of the ASIC the
 assembly temperature stabilized around 45°C .

In order to increase the probability to detect a photon
 an integration time of $1 \mu\text{s}$ was used. For this integra-
 tion time the leakage current of the sensor is no longer
 negligible and a higher noise than previously reported for
 100 ns integration time [13] was observed. A more detailed
 description of the operating conditions and their influence
 on the measurement results can be found in literature [13].
 A total of 5×10^5 frames were acquired. For comparison
 with the simulations only events of a single pixel were eval-
 uated⁵.

¹As this study focuses on very low photon count rates the term
 one photon is used as synonym for one or more photons, unless stated
 otherwise.

²At the investigated energy range possible primary interactions
 are (in order of decreasing likelihood): photoabsorption, coherent
 scattering and incoherent scattering. The probabilities of other in-
 teractions are many orders of magnitude lower.

³ISO DEBYEFLEX 3003 from GE Measurement and Control So-
 lutions, set to 50 kV and 39 mA

⁴99.9% from Goodfellow GmbH, 61213 Bad Nauheim, Germany

⁵In this way pixel to pixel variations are excluded from the com-
 parison

Window type	Aluminum [μm]	n^+ implantation [μm]	sensitive thickness [μm]
standard	0.5	1.2	497.6
thin	0.1	0.1	498.7

Table 1: Entrance windows investigated in this study, neglecting thin SiO_2 layers. The thickness of the sensor is 500 μm , where the last 1.2 μm are assumed to be insensitive due to the p^+ implantation.

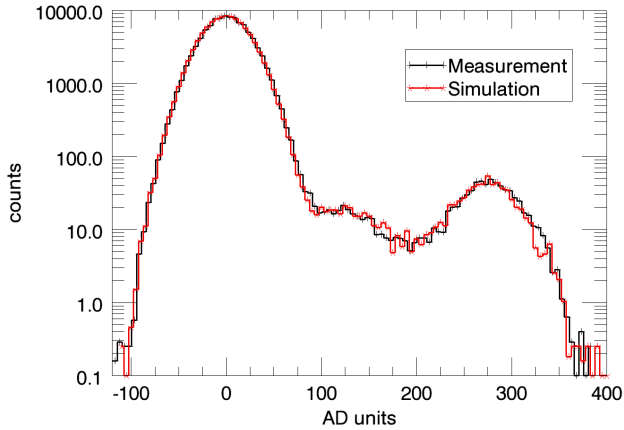


Figure 1: Comparison of measurements performed using AGIPD02 with sensor to a corresponding simulation with HORUS. 5 AD units have been binned together to reduce the apparent spread. Measurement and simulation match very well.

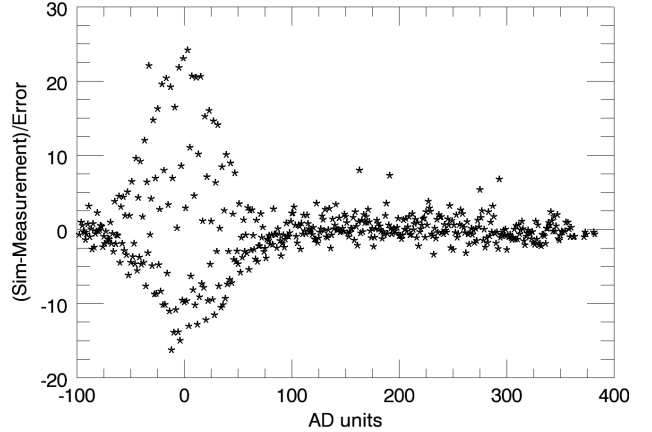


Figure 2: Difference between simulation and measurement in units of the measurement error (square root of the number of counts). The systematic deviations around the noise pedestal (0 AD units) are caused by fixed pattern noise in the readout system. Values above approximately 100 AD units show the expected statistical spread.

The corresponding HORUS simulations calculated one frame of 5×10^5 pixels, with an average probability (Poisson distributed) to have molybdenum and copper fluorescence photons impinge on a pixel of 2.22% and 0.193%. The fluorescence photons included K_α and K_β lines. The total equivalent noise charge (ENC) at the input of the simulated system was 405 electrons, in order to account for the mode of operation mentioned above.

Figure 1 shows a direct comparison of the measured and simulated counts as a function of AD (Analog to Digital converter) units using a semi logarithmic scale for better visibility of the small number of photon events. For operation at the European XFEL the AD units would have to be quantized to an integer number of photons, as detailed later in this manuscript.

Figure 2 shows the difference between simulation and measurement in units of the measurement error (square root of the number of counts). A perfect match with an infinite number of samples would show samples of a normal distribution with an rms (root-mean-square) value of $\sqrt{2}$ and a vanishing mean⁶. As observed from figure 2 there are some systematic deviations around the noise pedestal (0 AD units) caused by fixed pattern noise in the readout system. The fixed pattern noise shows an oscillatory behavior around the mean. Possible reasons for this include the pickup of external periodic signals and non equal bin sizes in the lower significant bits of the ADC. Evaluating

⁶A value of $\sqrt{2}$ and not 1.0 is expected as two independent random processes, measurement and simulation, are involved.

only values above 100 AD units results in an rms value of about 1.6 and a mean of 0.14, which are very close to the ideal values.

All in all the measurement data is reproduced very well. The fact that both K_α and K_β lines had to be included in the simulated spectrum to produce matching results shows the chosen method is suitable for the validation of the simulation package.

4.2. Quantum efficiency

The quantum efficiency QE can be approximated as the probability of a photon to be absorbed⁷ in the sensitive volume of the sensor as a function of photon energy E and angle θ between the incoming photon and the beam axis:

$$QE(E, \theta) = P_1(E, \theta) * P_2(E, \theta), \quad \text{with} \quad (2)$$

$$P_1(E, \theta) = \prod_i e^{-\frac{\mu_i(E)d_i}{\cos \theta}} \quad \text{and} \quad (3)$$

$$P_2(E, \theta) = 1 - e^{-\frac{\mu_{sens}(E)d_{sens}}{\cos \theta}}. \quad (4)$$

P_1 is the product of the transmission probabilities of all i materials of the entry window. It denotes the probability of a photon passing through the entry window without

⁷All derivations in this paragraph use the cross section for photoabsorption. As a consequence 2nd order effects including in-sensor scattering are neglected.

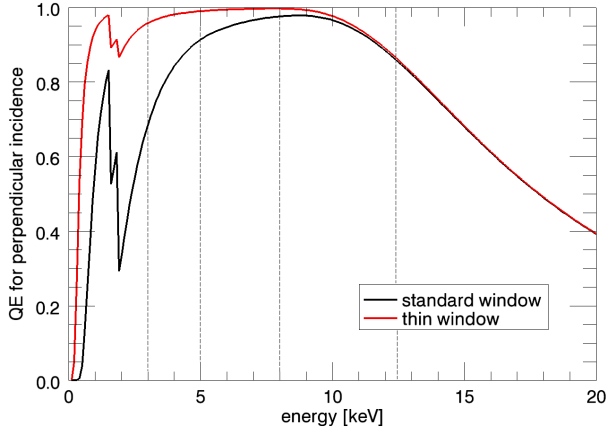


Figure 3: Approximate quantum efficiency as a function of energy for the two different window designs. The thin window significantly improves the QE for energies below approximately 5 keV. The vertical dashed lines indicate the energies investigated in this study.

interacting. μ_i and d_i are the linear attenuation coefficient and the thickness of material i taken from [14]. For the chosen sensor thickness P_1 is the dominating term at energies below approximately 8 keV.

P_2 denotes the probability of a photon being absorbed in the sensitive volume (dominating at energies above approximately 8 keV), with μ_{sens} and d_{sens} being the linear attenuation coefficient and the thickness of the sensitive material (silicon).

This approximation neglects any effects due to the finite lateral extent of the sensor material and any disturbances along the photon's flight path, especially all windows of vacuum vessels and flight tubes.

Reducing the thickness of the entry window materials has been suggested as a possibility to increase the sensitivity of AGIPD to low energy photons. A comparison of the material thicknesses of a standard window and a possible thin window is listed in table 1. The effect of a thin (few nm thickness) SiO_2 layer between aluminum and n^+ implantation is negligible. Details on the pixel layout and junction depth on the readout side can be found in literature [15].

The results for the quantum efficiency for both windows as a function of energy are shown in figure 3. A thin window would increase the QE compared to the standard window by about 40%, 7%, 2% and 1% at an energy of 3, 5, 8 and 12.4 keV, respectively.

5. Estimated performance of AGIPD

Measurements of AGIPD02 showed an overall ENC of approximately 400 electrons. The dominant noise contributions originate in the Correlated Double Sampling (CDS) stage and the readout buffer. These parts of the ASIC circuitry have been modified to have a lower noise contribution and were manufactured on other test chips

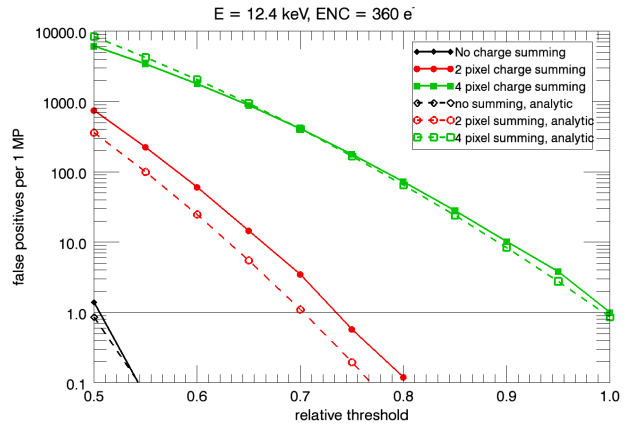
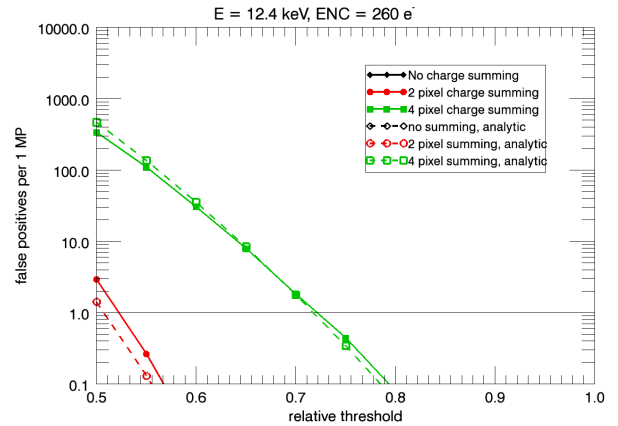


Figure 4: Number of false positives in a 1 MP detector for an ENC of 260 electrons (top) and 360 electrons (bottom) as a function of relative threshold and charge summing scheme. Values below 0.1 false positive per frame are not displayed. Without charge summing at an ENC of 260 electrons the false positive rate is consistently below 0.1.

(AGIPD03 and AGIPD04). Measurements of these test chips are currently performed, but not yet available.

Circuit simulations of the improved parts allow an estimation of the total noise to be around 270 electrons for AGIPD03, and a reduced noise was verified by preliminary measurements of the chip. The AGIPD04 test chip features one pixel column with an increased gain in the first gain stage, which might reduce the total noise in this column to 230 electrons⁸.

Assuming that these results and expectations are transferable to AGIPD10, a full scale chip featuring 64×64 pixels, one can estimate the ENC of the system to be between 200 and 400 electrons. Selected simulations with 260 and 360 electrons ENC will be presented in more detail.

5.1. Single photon sensitivity

The single photon sensitivity, as defined in the introduction ($P(1|0) < 10^{-6}$ and $\bar{P}(1|1) > 0.5$), is a function

⁸As CDS stage and readout buffer insert their noise 'downstream' of the preamplifier an increase in gain reduces the equivalent noise charge on the input.

228 of the systems noise and the threshold used for data eval-
 229 uation. The threshold is restricted to the interval from
 230 $0.5E_\gamma$ to E_γ , as lower thresholds result in significant double
 231 counting of events and higher thresholds have $\bar{P}(1|1) < 0.5$
 232 by definition. This manuscript will present all threshold
 233 dependencies relative to the beam energy E_γ .

234 The absolute simulation error was estimated to be less
 235 than 10^{-8} for $P(1|0)$ (1 false positive in 100 frames of
 236 1MP⁹ each) and better than 10^{-7} for the other shown
 237 parameters (defined later).

238 All results are normalized to the number of photon
 239 interactions in the sensitive layer.¹⁰ In order to normalize
 240 to the number of incident photons the results have to be
 241 multiplied with the quantum efficiency QE (shown as a
 242 function of energy in figure 3).

243 5.2. Design energy: 12.4 keV

244 As shown in figure 4, less than one false positive per
 245 1 MP can be achieved throughout the entire investigated
 246 noise range. It is not shown, but the true positive rate for
 247 low thresholds is close to the theoretical maximum value of
 248 approximately 97%¹¹. For larger thresholds the detection
 249 efficiency drops a little but stays above 50%, similar to the
 250 behavior shown in upper image in figure 6, which will be
 251 discussed in more detail later. Therefore single photon
 252 sensitivity at 12.4 keV beam energy is achieved.

253 In most of the investigated noise range single photon
 254 sensitivity can also be obtained when using charge sum-
 255 ming schemes. The details of the used summing algorithm
 256 and why 2 pixel summing produces more false positives
 257 than analytically expected and 4 pixel summing produces
 258 sometimes more and sometimes less is explained in ap-
 259 pendix Appendix A. It should be noted that charge sum-
 260 ming is a data processing step which is done offline, i.e. not
 261 within the ASIC¹², as done e.g. in the Medipix3 chip[16].

262 The impact of charge summing is detailed in the next
 263 paragraph using an example of 8 keV photons and low
 264 noise.

265 5.3. Reduced beam energy: 8 keV

266 Figure 5 shows the situation for a beam energy of 8 keV
 267 and no charge summing. Single photon sensitivity can be
 268 achieved over the whole investigated noise interval (not
 269 shown). Charge summing, however, can only be applied
 270 at low noises if single photon sensitivity shall be kept (see
 271 figure 6).

272 The situation for high noise levels is very similar to
 273 the situation for low noise levels and 5 keV beam energy,

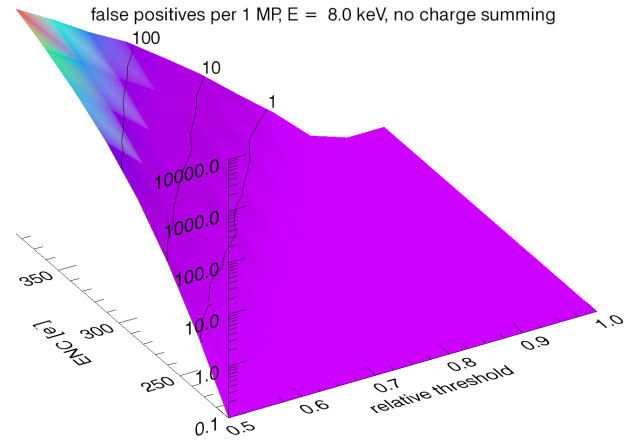


Figure 5: False positives in a 1 MP detector as a function of noise and relative threshold. Values below 0.1 false positive per frame are not displayed.

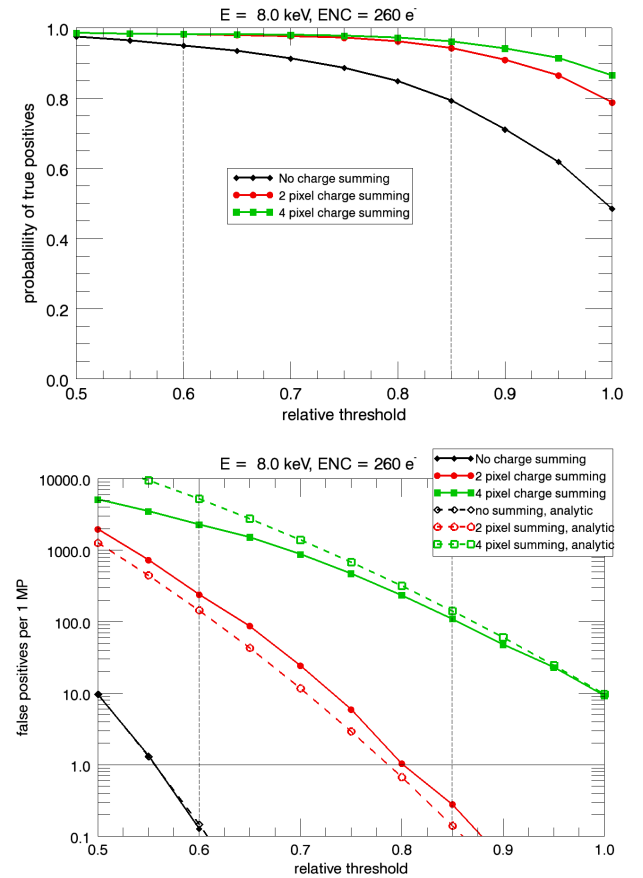


Figure 6: True and false positive rates in a 1 MP detector for a fixed ENC of 260 electrons as a function relative threshold and charge summing scheme. The thresholds needed to reduce the false positives to less than 1 per MP are indicated by the dashed lines.

which is detailed in the next paragraph. The situation for low noise is detailed here.

Figure 6 shows the true and false positive rate for a fixed ENC of 260 electrons. If $P(1|0) < 10^{-6}$ is required,

⁹1 MP indicates a frame of $1024 \times 1024 \approx 10^6$ pixels.

¹⁰In this way the results are independent of the photon energy.

¹¹The theoretical maximum value of the probability to detect a true positive is not unity, as there is about 3% probability of a photon scattering and being absorbed in a different pixel at this energy.

¹²It would be possible to include the data processing at some point in the readout chain, but this is not foreseen at the moment.

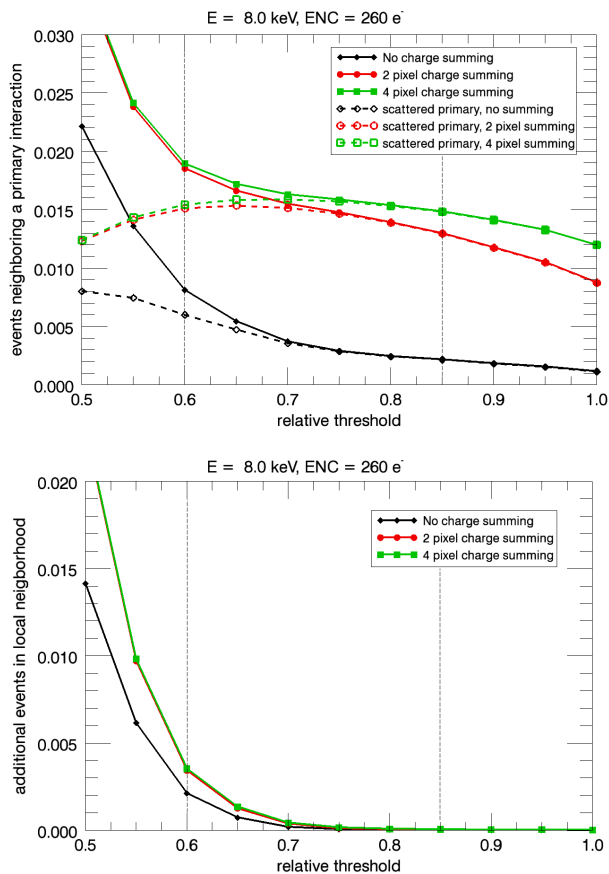


Figure 7: The upper image shows the expected number of events above threshold in the eight pixels surrounding the pixel where a primary interaction took place (solid lines) and the contribution of these events which are photoabsorption of a photon scattered in the primary event (dashed lines). The lower image shows the average number of excess events a primary photon produces. The thresholds needed to reduce the false positives to less than 1 per MP are indicated by the dashed lines.

the relative threshold has to be increased to approximately 0.6, when no charge sharing scheme is used and to approximately 0.85 when the 2 pixel summing scheme is used. At these thresholds the true positive rate is approximately 95% for both.

The benefit of employing charge summing is shown in figure 7. The upper image shows the expected number of events above threshold in the eight pixels surrounding the pixel where a primary interaction took place (solid lines) and the contribution of these events which are photoabsorption of a photon scattered in the primary event (dashed lines). The lower image shows the 'additional events', i.e. the average number of excess events a primary photon produces (which is the difference between the solid and dashed lines in the upper image).

For the thresholds mentioned above, using 2 pixel charge summing reconstructs 0.7% more events (difference of the dashed lines in the upper plot of figure 7) than no charge summing scheme, although these events are displaced by

false positives per 1 MP, E = 5.0 keV, no charge summing

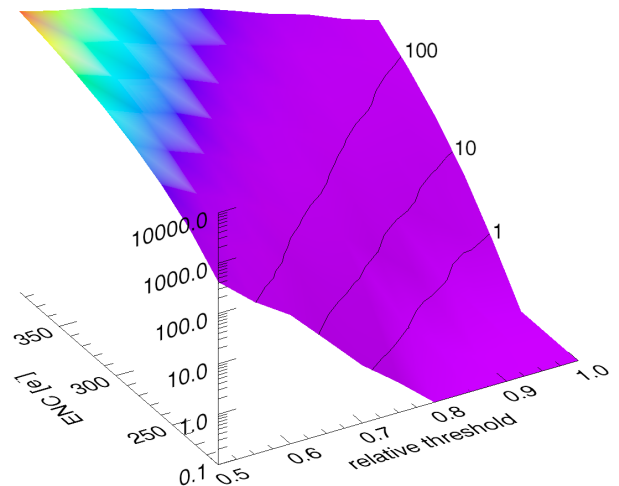


Figure 8: False positives in a 1 MP detector as a function of noise and relative threshold. Values below 0.1 false positive per frame are not displayed.

1 pixel from the primary interaction.

Not using charge summing results in 0.2% additional events in the local neighborhood, i.e. every 500th event is counted as two events in adjacent pixels. When using 2 pixel charge summing only approximately 5×10^{-5} events (1 every 20'000) are counted as two events. This is a reduction by a factor of 40.

At an ENC of 360 electrons the results are similar to the results obtained for 5 keV energy and an ENC of 260 electrons, which are discussed below.

5.4. Extended energy range: 5 keV

For a beam energy of 5 keV single photon sensitivity can be achieved in a low noise scenario, as shown in figure 8 and 9. At an ENC of 260 electrons a relative threshold of 0.9 has to be selected to achieve single photon sensitivity, which in turn leads to an average true positive rate of approximately 63% (see figure 9).

At high relative thresholds $P(1|1)$ is no longer uniform over the pixel area, but decreases strongly towards the edges and corners of a pixel as a result of the extend of the charge cloud generated by the individual x-rays. The simulation of a microbeam scan visualizing this effect is shown in figure 10. While in the central region of a pixel $P(1|1)$ is approximately 80%, it decreases sharply towards a pixels edge, vanishing almost completely at the corner. The microbeam scan used a square beam with a size of $(10 \mu\text{m})^2$ and an energy of 5 keV. The origin of the coordinate system is centered on the pixel corner, and any event registered by one of the four pixels is counted.

5.5. Low energy operation: 3 keV

Single photon sensitivity, as defined in this work, cannot be achieved at 3 keV beam energy. The average count rate of false 'hits' is below 0.035 per pixel per frame (see

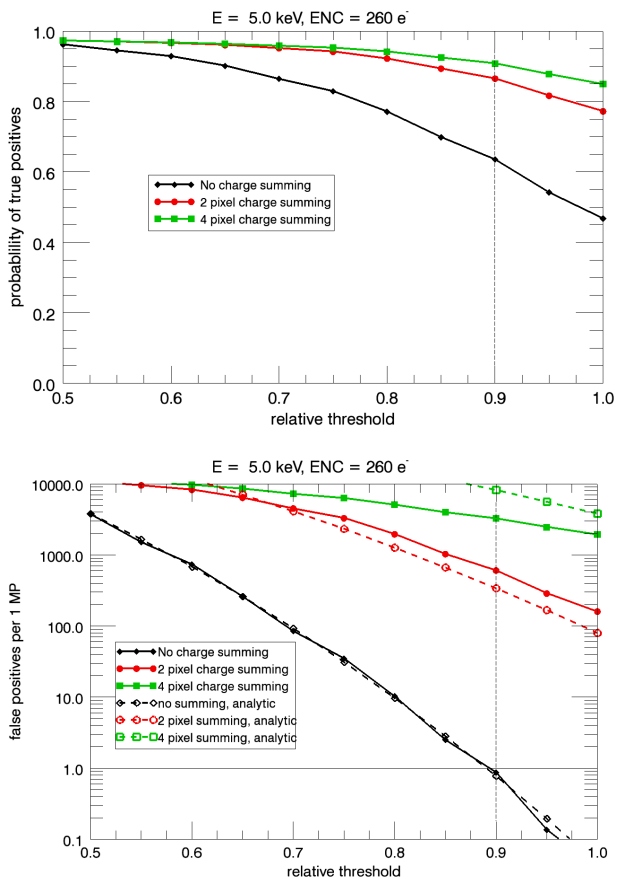


Figure 9: True and false positive rates in a 1 MP detector for a fixed ENC of 260 electrons as a function relative threshold and charge summing scheme. The threshold needed to reduce the false positives to less than 1 per MP is indicated by the dashed line.

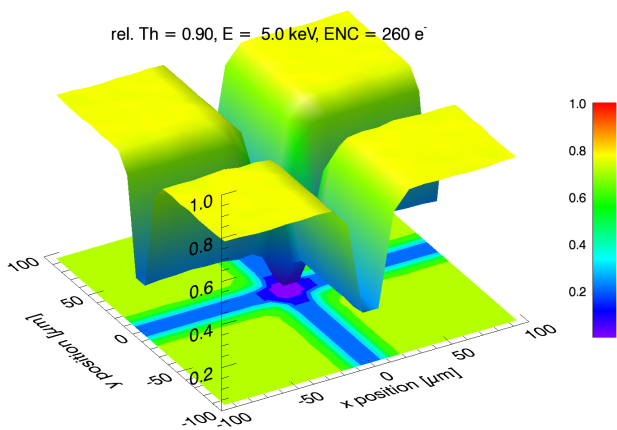


Figure 10: Microbeam scan using a beam size of $(10 \mu\text{m})^2$ and a beam energy of 12.4 keV in the entire investigated noise regime, and at 5 keV. The origin of the coordinate system is centered on the pixel corner.

figure 11, depending on noise and threshold a reduction by a factor > 10 can be achieved), but significantly above the required 10^{-6} . Due to the Gaussian nature of the noise no more than 1 or 2 'false' photons will be detected in an individual pixel, depending on ENC and threshold.

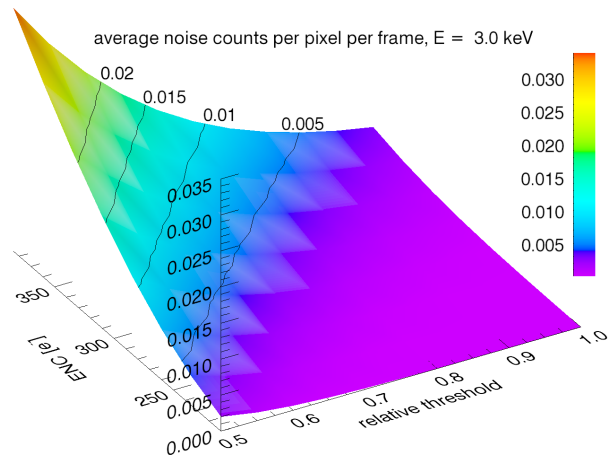


Figure 11: Average number of photon 'hits' due to noise per pixel per frame as a function of noise and relative threshold.

Even though single photon sensitivity is not given, imaging at this energy is still possible. When the relative threshold is chosen below 0.7, the average probability to detect an impinging photon is above 70%, allowing Poisson noise limited performance for signals significantly above the noise floor.

6. Summary

This work investigated the single photon sensitivity of the AGIPD detector. Single photon sensitivity was defined as the possibility to select a threshold such that the expected rate for false positives is below one per frame ($P(1|0) < 10^{-6}$), while simultaneously having an average true positive rate of more than 50% ($\bar{P}(1|1) > 0.5$).

Simulations were performed using the HORUS detector simulation toolkit, assuming the noise of the final AGIPD to lie in the interval between 200 and 400 electrons.

It was shown that AGIPD is single photon sensitive throughout the investigated noise interval down to 8 keV beam energy. Should the final noise be at the lower end of the possible range (e.g. 250 electrons) single photon sensitivity can also be achieved at 5 keV beam energy.

It was shown that charge summing schemes are beneficial when the noise is sufficiently low. The total detection rate of events increased (although some of the events were reconstructed in neighboring pixels) and the possibility to count one event twice in adjacent pixels is reduced by a factor of 40. Charge summing can be used at the design energy, and at 8 keV if the noise is low (e.g. 250 electrons).

The low energy performance of AGIPD was explored, finding a noise floor below 0.035 'hits' per pixel per frame at 3 keV beam energy. Even though single photon sensitivity, as defined in this work, is not given, imaging at this energy is still possible, allowing Poisson noise limited performance for signals significantly above the noise floor.

Appendix A. Applied charge summing algorithm

Summing the response of two or more pixels is a way to recombine energy depositions which were spread over adjacent pixels, thereby reconstructing the initial photon energy.

As pixels are summed up, so is their noise. Assuming the noise of all pixels to be uncorrelated and to have an identical rms value of ENC , the N binned pixels can be considered one larger pixel with a noise of $\sqrt{N} ENC$. This value and equation 1 were used as an estimate of the expected noise, as shown in figures 4, 6 and 9.

In the present study pixels were not binned unconditionally but had to fulfill certain criteria:

- Pixels were considered suitable for summing when their energy deposition exceeded 570 electrons¹³ (approximately 2 keV), but was below threshold (seed criterion).
- 2 pixel summing: Pixels fulfilling the seed criterion and being above threshold when summed with one of their four direct neighbors were considered hit, when their energy contribution was largest (neighbor criterion). If more than one possibility to fulfill the neighbor criterion was found, the pixels with the highest total energy deposition were summed. Pixels could only be summed once.
- 4 pixel summing: Pixels fulfilling the seed criterion, but not the neighbor criterion had the neighbor criterion extended to 2 by 2 pixel regions (Quad criterion).

As the pixels were not summed unconditionally, the introduced selection bias increases the probability of finding a false positive beyond the expected $\sqrt{2} ENC$ for unconditional 2 pixel summing¹⁴. On the other hand the introduced selection bias sometimes decreased the probability of finding a false positive below the expected $2 ENC$ for unconditional 4 pixel summing, as summing two pixels fulfilled the neighbor criterion for most pixels.

References

- [1] M. Altarelli et al., European X-ray Free Electron Laser. Technical Design Report, ISBN 978-3-935702-17-1 (2006).
- [2] Th. Tschentscher et al., Layout of the X-Ray Systems at the European XFEL, TECHNICAL NOTE XFEL.EU TN-2011-001 (2011).
- [3] B. Henrich et al., The adaptive gain integrating pixel detector AGIPD a detector for the European XFEL, Nucl. Instr. and Meth. A, DOI: 10.1016/j.nima.2010.06.107.

- [4] X. Shi et al., Challenges in chip design for the AGIPD detector, Nucl. Instr. and Meth. A 624(2) 2010 387-391, DOI: 10.1016/j.nima.2010.05.038.
- [5] G. Potdevin et al., Performance simulation of a detector for 4th generation photon sources: The AGIPD, Nucl. Instr. and Meth. A 607(1) 2009 51-54, DOI: 10.1016/j.nima.2009.03.121.
- [6] A. Mancuso et al., Conceptual Design Report: Scientific Instrument SPB, 2011, TR-2011-007
- [7] A. Madsen et al., Conceptual Design Report: Scientific Instrument MID, 2011, TR-2011-008
- [8] G. Potdevin, U. Trunk, H. Graafsma, HORUS, an HPAD X-ray detector simulation program, J. Inst. 4 2009 P09010, DOI: 10.1088/1748-0221/4/09/P09010.
- [9] D. Pennicard, et al., Simulations of charge summing and threshold dispersion effects in Medipix3, Nucl. Instr. and Meth. A 636(1) 74-81, DOI: 10.1016/j.nima.2011.01.124.
- [10] D. Pennicard and H. Graafsma, Simulated performance of high-Z detectors with Medipix3 readout, J. Inst. 6 2011 P06007, DOI: 10.1088/1748-0221/6/06/P06007.
- [11] G. Potdevin, H. Graafsma, Analysis of the expected AGIPD detector performance parameters for the European X-ray free electron laser, Nucl. Instr. and Meth. A, DOI: 10.1016/j.nima.2011.09.012.
- [12] J. Becker, C. Gutt, H. Graafsma, Simulation study of the impact of AGIPD design choices on X-ray Photon Correlation Spectroscopy utilizing the intensity autocorrelation technique, J. Inst. 6 2011 P11005 doi:10.1088/1748-0221/6/11/P11005.
- [13] D. Greiffenberg, The AGIPD detector for the European XFEL, J. Inst. 7 2012 C01103 doi:10.1088/1748-0221/7/01/C01103
- [14] C. T. Chantler et al., Detailed Tabulation of Atomic Form Factors, Photoelectric Absorption and Scattering Cross Section, and Mass Attenuation Coefficients for $Z = 1-92$ from $E = 1-10$ eV to $E = 0.4-1.0$ MeV, J. Phys. Chem. Ref. Data 29(4), 597-1048 (2000), updated electronic version available at the NIST webpage <http://www.nist.gov/pml/data/ffast/index.cfm>
- [15] J. Schwandt et al., Optimization of the Radiation Hardness of Silicon Pixel Sensors for High X-ray Doses using TCAD Simulations, arXiv:1111.4901v1
- [16] R. Ballabriga, M. Campbell, E. Heijne, X. Llopart, and L. Tlustos, The Medipix3 prototype, a pixel readout chip working in single photon counting mode with improved spectrometric performance, Nuclear Science, IEEE Transactions on, vol. 54, pp. 1824 -1829, oct. 2007

¹³The seed criterion reduces the number of possible pixel summing combinations to test. As long as it is below half, resp. one quarter, of the beam energy it has no influence on the result.

¹⁴An example is a pixel being just above threshold with all its neighbors being negative enough for the sum to be below threshold. Unconditional summing will not detect a hit, while the employed summing algorithm will.